Biochimica et Biophysica Acta 1861 (2016) 594–605

Contents lists available at ScienceDirect

Biochimica et Biophysica Acta

journal homepage: www.elsevier.com/locate/bbalip

Cellular cholesterol accumulation modulates high fat high sucrose (HFHS) diet-induced ER stress and hepatic inflammasome activation in the development of non-alcoholic steatohepatitis

Amir Bashiri [a,b], Dinushan Nesan [a], Ghazaleh Tavallaee [a], Ian Sue-Chue-Lam [a], Kevin Chien [a], Graham F. Maguire [a], Mark Naples [e], Jing Zhang [e], Lilia Magomedova [d], Khosrow Adeli [e], Carolyn L. Cummins [d], Dominic S. Ng [a,b,c,*]

[a] Keenan Research Centre, Li Ka Shing Knowledge Institute, Department of Medicine, St Michael's Hospital, Toronto, Canada
[b] Department of Physiology, Faculty of Medicine, University of Toronto, Toronto, Canada
[c] Department of Laboratory Medicine and Pathobiology, University of Toronto, Toronto, Canada
[d] Faculty of Pharmacy, University of Toronto, Toronto, Canada
[e] Molecular Structure and Function Program, Research Institute, The Hospital for Sick Children, Toronto, Ontario, Canada

ARTICLE INFO

Article history:
Received 9 November 2015
Received in revised form 5 April 2016
Accepted 11 April 2016
Available online 14 April 2016

Keywords:
NASH
ER cholesterol
ER stress
Inflammasome
Cholesterol crystal
LCAT knockout mice

ABSTRACT

Non-alcoholic steatohepatitis (NASH), is the form of non-alcoholic fatty liver disease posing risk to progress into serious long term complications. Human and pre-clinical models implicate cellular cholesterol dysregulation playing important role in its development. Mouse model studies suggest synergism between dietary cholesterol and fat in contributing to NASH but the mechanisms remain poorly understood. Our laboratory previously reported the primary importance of hepatic endoplasmic reticulum cholesterol (ER-Chol) in regulating hepatic ER stress by comparing the responses of wild type, *Ldlr* −/−*xLcat* +/+ and *Ldlr* −/−*xLcat* −/− mice, to a 2% high cholesterol diet (HCD). Here we further investigated the roles of ER-Chol and ER stress in HFHS diet-induced NASH using the same strains. With HFHS diet feeding, both WT and *Ldlr* −/−*xLcat* +/+ accumulate ER-Chol in association with ER stress and inflammasome activation but the *Ldlr* −/−*xLcat* −/− mice are protected. By contrast, all three strains accumulate cholesterol crystal, in correlation with ER-Chol, albeit less so in *Ldlr* −/−*xLcat* −/− mice. By comparison, HCD feeding per se (i) is sufficient to promote steatosis and activate inflammasomes, and (ii) results in dramatic accumulation of cholesterol crystal which is linked to inflammasome activation in *Ldlr* −/−*xLcat* −/− mice, independent of ER-Chol. Our data suggest that both dietary fat and cholesterol each independently promote steatosis, cholesterol crystal accumulation and inflammasome activation through distinct but complementary pathways. In vitro studies using palmitate-induced hepatic steatosis in HepG2 cells confirm the key roles by cellular cholesterol in the induction of steatosis and inflammasome activations. These novel findings provide opportunities for exploring a cellular cholesterol-focused strategy for treatment of NASH.

1. Introduction

Non-alcoholic fatty liver disease (NAFLD) is one of the most common chronic liver disorders that encompass a spectrum of clinical manifestations from simple steatosis to steatosis with necroinflammation, or non-alcoholic steatohepatitis (NASH). The presence of NASH is known to predispose to the progression to fibrosis, cirrhosis and hepatocellular carcinoma [1–3]. In humans, a histopathological diagnosis of NASH entails the concurrent presence of lobular inflammation and cytologic ballooning [4], the latter being strongly correlated with elevated cellular cholesterol and insulin resistance [5,6]. A lack of easily accessible clinical biomarkers makes full understanding of the pathogenesis, especially the transition from simple steatosis to NASH particularly challenging.

Classically, fatty acid dysregulation has been regarded as the central driver of NAFLD [7,8]. Recent studies increasingly recognize cholesterol dysregulation playing an important role [9]. Lipidomic analyses revealed accumulation of tissue free cholesterol level, disproportional to that of cholesterol ester in NAFLD subjects [10]. Min et al. further reported coordinated alterations in several cholesterol homeostatic pathways in favor of net free cholesterol accumulation [6]. The pathogenesis of this profile of cholesterol dysregulation and their role in NASH remain incompletely understood.

A number of pre-clinical models identified a synergistic effect between dietary cholesterol and saturated fat, in the development of

* Corresponding author at: Keenan Research Center, St. Michael's Hospital, 30 Bond St, Shuter 3-041, Toronto, ON M5B1W8, Canada.
E-mail address: ngd@smh.ca (D.S. Ng).

http://dx.doi.org/10.1016/j.bbalip.2016.04.005
1388-1981/

NASH. A 30-week feeding with either a 1% cholesterol/low fat (4%) or a high fat diet (15% fat without cholesterol) induces simple steatosis but the combined diet led to a marked acceleration of inflammation and fibrosis [11]. A similar cholesterol- and fat-rich diet murine model also demonstrated activation of Kupffer cells in the engulfing of cholesterol crystal-enriched lipid droplets from dead hepatocytes [12,13]. In LDL receptor knockout mice, feeding with a combined high fat high cholesterol diet for 3 months resulted in sustained steatohepatitis and fibrosis and intriguingly, omission of cholesterol in this diet resulted in selective inhibition of the inflammatory component without affecting the steatosis [14]. The mechanism underlying this synergistic effect is not well understood. While high fat diet feeding per se has been shown to induce endogenous hepatocyte cholesterol biosynthesis [15–17]; the relative importance of dietary fat-induced endogenously synthesized cholesterol, versus that from dietary cholesterol uptake towards NASH development and the mechanism for the synergistic effect of the two ingredients remain unclear and warrant further investigation.

Endoplasmic reticulum stress has been causally linked to activation of inflammasome in a number of tissue specific diseases. For example, hyperglycemia induced ER stress promotes NLRP3 inflammasome activation in pancreatic β cells via thioredoxin interacting protein [18] in the development of β cell dysfunction. ER stress has been implicated to play a role in NAFLD but its role in NLRP3 inflammasome activation has not been adequately addressed [9].

In order to address the potential roles of dietary cholesterol and its putative interaction with dietary fat in the pathogenesis of NASH, we employed three mouse strains, namely C57Bl/6 wild type (WT), LDL receptor knockout (*Ldlr −/−xLcat +/+*, SKO) and LDL receptor/lecithin cholesterol acyltransferase (LCAT) double knockout (*Ldlr −/− xLcat −/−*, DKO). LCAT plays a key role in mediating the esterification of free cholesterol (FC) in circulating lipoproteins and the complete absence of this enzyme results in not only profound alteration of lipoprotein composition and levels, but also cellular cholesterol homeostasis [19,20]. By examining the differential responses from these three mouse strains, to either regular chow or a 2% high cholesterol diet (HCD), we identified a selective dependency of hepatic ER stress on ER cholesterol—but not directly in other compartments [20]. This finding was based on the unexpected observation that the DKO mice being protected from ER cholesterol accumulation and ER stress in spite of excess cholesterol build-up in non-ER compartments in response to the diet. Herein, we utilized the same strains of mice to test the hypothesis that de novo cholesterol biosynthesis in response to high fat high sucrose (HFHS) diet alone is sufficient to induce hepatic ER cholesterol (ER-Chol) accumulation, ER stress and NLRP3 inflammasome activation. We also explored the differential impact of HFHS diet [21] and HCD on ER stress, inflammasome activation and development of NASH. We observed that dietary cholesterol can induce hepatic NLRP3 inflammasome activation independent of ER-Chol and ER stress.

2. Materials and methods

2.1. Reagents

Sodium palmitate (Pal), zaragozic acid (ZA), cholesterol, dimethyl sulfoxide (DMSO) and methyl-β-cyclodextrin (MCD) were purchased from Sigma Aldrich, Oakville, ON.

2.2. Animals

Ldlr −/−xLcat +/+ and *Ldlr −/−xLcat −/−* mice in C57Bl/6 background were generated as described previously [20,21]. WT mice were purchased from the Jackson Laboratory, Bar Harbor, ME and used as controls. Age matched female animals were used in all experiments. Ten week old female mice were fed a high fat high sucrose (HFHS) diet (Bio-Serv F3282, Flemington, NJ) [21] with 36% fat and no cholesterol for 16 weeks, a diet also known as high fat diet in other studies [22,23]. Another set of mice were fed a 2% high cholesterol diet (HCD) as previously described [20] for 10 weeks. Age-matched female mice fed a regular chow were diet used as controls. Mice were fasted for 12 h prior to sacrifice. The liver tissues were divided to different sections for storage at −80 °C for RNA, protein and lipid analysis. All experimental procedures used were approved by the Animal Care Committee at St. Michael's Hospital, Toronto, ON.

2.3. Cell culture

Human hepatocellular carcinoma cells (HepG2) were kind gifts from Dr. Khosrow Adeli's laboratory, Toronto, ON. Cells were cultured in Dulbecco's Modified Eagle's Medium (DMEM) (ATCC, Manassas, VI), supplemented with 10% fetal bovine serum albumin (FBS) (Life Technologies, Burlington, ON) and 1% penicillin/streptomycin (Sigma Aldrich, Oakville, ON) in a humidified atmosphere containing 5% CO_2 at 37 °C. The cells were starved in serum-free DMEM for 24 h prior to treatment in the presence or absence of zaragozic acid (ZA). Palmitate was conjugated with bovine serum albumin (BSA), essentially free of fatty acids (Sigma Aldrich, Oaville, ON) in a 6:1 ratio (Palmitate:BSA) following a protocol by Seahorse Bioscience (North Billerica, MA) and added to the cells at 0.3 mM. Zaragozic acid was prepared in DMSO and kept on ice until immediately before use and added at 10 μM. Cholesterol was conjugated with methycyclodextrin (MCD) as described previously and added at 5, 10 and 20 μg/ml [20].

2.4. mRNA quantitation of hepatic genes

RNA extraction, generation of cDNA and quantitative RT-PCR from liver tissue or HepG2 cells were carried out as described previously [20]. Briefly, mRNA was isolated using a modified phenol-chloroform extraction using Trizol reagent (Life Technologies, Burlington, ON). First-strand cDNA synthesis was carried out using the Qiagen Quantitect Reverse Transcription Kit (Toronto, ON) according to manufacturer's protocols. qPCR analysis was performed in 384-plates using a Viia 7 Real-Time PCR system with SYBR Select Master Mix (both from Life Technologies). The PCR reaction involved denaturation at 95 °C for 10 min, followed by 40 cycles of amplification at 95 °C for 15 s and 62 °C for 1 min. Fluorescence measurements were made in each cycle at 494–521 nm. The relative mRNA expression was determined using the comparative Ct method by calculating $2^{-\Delta\Delta Ct}$ [24]. The primers were synthesized by the DNA Synthesis Facility at the Hospital for Sick Children (Toronto, ON). The expression of *Xbp1s*, *Chop*, *Nlrp3*, *Sqs*, *Srebp2*, *and Pro-Il-1β* was analyzed by quantitative RT-PCR and glyceraldehyde-3-phosphate dehydrogenase (*Gapdh*) was used as an internal control. Mouse and human primer pairs used to amplify these genes were as follows (forward and reverse, respectively): mouse *Chop* 5′-*ctgcctttcaccttggagac*, 5′-*tataggtgccccccattttca*; mouse *Hmgr* 5′-*tctggcagtcagtgggaactatt*, 5′-*cctcgtccttcgatccaattt*; mouse *Gapdh* 5′-*acccagaagactgtggatgg*, 5′-*ggatgcagggatgatgttct*; mouse *Sqs* 5′-*taag cctgctgcgtatgttg*, 5′-*cccagtaatccagcaaggaa*; mouse *Xbp1s* 5′-*gagtcc gcagcaggtg*, 5′-*gtgtcagagtccatggga*, mouse *Nlrp3* 5′-*tagtgattggcagcaggtct*, 5′-*tggggtatctgggatgttta*, mouse *pro-Il-1β*: *5-tcgctcagggtcacaagaaa-3*, *5-atcagaggcaaggaggaaacac-3*; human *CHOP 5′-ctcttgaccctgcttctctg-*, 5′-*cactcttgaccctgcttctc*; human *HMGR 5′-gcacagaatgttggtagttcaa-*, *5′-ctt gctgaggtagtaggttggt*; human *GAPDH 5′-cccatgttcgtcatgggtgt-*, *5′-ata ccatgagtccttccacgata*; human *SQS* 5′-*ggtcccgctgttacacaact*, *5′-aaaa ctctgccatcccaatg*; human *XBP1s 5′-ccgcagcaggtgcagg, 5′-gagtcaata ccgccagaatcca.*

2.5. Western blot analysis

Liver tissue or treated HepG2 cells were extracted for protein using radioimmunoprecipitation assay lysis buffer added with protease inhibitors (Santa Cruz Biotechnology, Santa Cruz, CA). Protein concentrations

in the supernatant were determined using a Bio-Rad protein assay kit. Rabbit monoclonal to CIAS1/NALP3 (NLRP3) (Abcam, Toronto, ON), rabbit polyclonal to IL-1β (Abcam, Toronto, ON), rabbit polyclonal to HMGR (Santa Cruz Biotechnology, Santa Cruz, CA) and SQS (GeneTex Inc., Irvine, CA), rabbit polyclonal to β-actin (Rockland, Limerick, PA) and mouse monoclonal to GAPDH (Abcam, Toronto, ON) were purchased. Western blots were carried out as described previously [21]. Briefly, 50 μg of protein was loaded for each treatment into a Criterion TGX Precast Gel (Bio-Rad, Mississauga, ON). The gel was run at 150 mV for 1 h and transferred onto nitrocellulose membrane using Bio-Rad Transblot Turbo (Mississauga, ON). The blots were incubated with primary antibodies at 1:1000 dilution overnight, with the exception of GAPDH, which was incubated at 1:15,000 dilution. The blots were then incubated for 1 h with respective secondary antibodies at 1:2000 dilution, with the exception of GAPDH, which was incubated at 1:10,000 dilution. The blots were incubated with enhanced chemiluminescence (ECL) (Life Technologies, Burlington, ON) substrate and developed on Thermo Scientific CL-Xposure Film (Fisher Scientific, Ottawa, ON).

2.6. Hepatic lipid analyses

Hepatic lipid analysis was carried out on liver tissue and HepG2 cells as described previously using a modified Folch lipid extraction [20]. Briefly, 100 mg of liver tissue was homogenized in 5 ml of 2:1 chloroform:methanol solution supplemented with 0.005% butylated hydroxytoluene (BHT, Sigma Aldrich). After centrifugation at 1500 g for 30 min, the lipid fractions were washed once with 50 mM NaCl, and twice with 1 ml 0.36 mM $CaCl_2$.The lipid fraction was then evaporated under N_2 flow and reconstituted in a fixed volume of chloroform containing 0.005% BHT. The levels of triglyceride and total cholesterol (Beckman Coulter, Mississauga, ON) and free cholesterol (Wako Diagnostics, Richmond, VI) were measured using colorimetric assays.

2.7. ER membrane lipid analysis

Endoplasmic reticulum (ER) was extracted and analyzed for its lipid content as described previously [20]. Briefly, ~100 mg of liver tissue was homogenized and centrifuged at 100,000*g* for 40 min, producing a crude membrane pellet, which was then resuspended in a sucrose solution and loaded onto a sucrose gradient. After ultracentrifugation at 100,000*g* for 1 h, the heavier membrane fraction (bottom) was further purified using iodixanol gradient at 110,000*g* for 2 h. The resulting gradient was collected in 12 fractions, which were tested by western blot against ACAT2 (Abcam, Toronto, ON). The ACAT2-positive fractions were pooled together and extracted for lipids as explained above. The cholesterol content was detected using LC/MS/MS, and the concentration of phospholipids was determined using an enzymatic assay kit (Wako Diagnostics).

2.8. LC/MS/MS analysis of ER cholesterol

The LC/MS/MS analysis was performed as described previously [20]. Briefly, lipid extracts described above were dissolved in 100% methanol and analyzed on a 6410 LC/MS/MS instrument (Agilent Technologies, Santa Clara, CA) with an electrospray ionization source in positive ion mode. Fifty microliter of sample was separated on a Zorbax-XDB C18 column (4.6 × 50 mm, 3.5 μm) by gradient elution at 0.4 ml/min. The mobile phase consisted of HPLC grade water (A) and methanol (B), both containing 5 mM ammonium acetate. The following gradient program was run: 0–1 min, 90% B; 1–3.3 min, 90–100% B; 3.3–20 min, 100% B. MS parameters were as follows: nebulizer pressure, 35 p.s.i.; drying gas (nitrogen), 10 l/min; capillary voltage, 4000 V; column temperature, 40 °C; drying gas temperature, 175 °C for all compounds. The following transitions were observed in multiple reaction monitoring mode: cholesterol-d_7 (m/z 411 → 376; retention time 12.5 min) and cholesterol (m/z 404 → 369; retention time 12.6 min). Fragmentor voltage was 105 V, and collision energy was 1 V. The cholesterol concentrations in each sample were then determined using the standard curve and normalized to the amount of internal standard present.

2.9. Liver histology

Liver tissues were embedded in 10% formaldehyde for 48 h.

For H&E analyses, the tissues were paraffin embedded and sectioned with a Leica RM2235 microtome. For the detection of cholesterol crystals, light microscopy with and without polarized filter was used to detect crystal birefringence as previously described [12,13]. Briefly, frozen tissues were embedded in optimal cutting temperature (OCT) (Fisher Scientific, Ottawa, ON) compound and frozen on dry ice. Frozen sections (10 μm in thickness) were prepared using a Leica CM1950 cryostat. The sections were mounted with glycerol. Imaging was performed using a Nikon Eclipse E800 microscope, Nikon DS-R3 camera, and Nikon's NIS-Elements software. Polarized light microscopy was used to identify cholesterol crystals by the presence of birefringence of the polarized light path. Images were processed using the Fiji build of ImageJ to threshold and count all pixels above an RGB intensity of 20 (up to the max of 255). The count of pixels above threshold was then generated as a percentage of total pixels, and that was used as a measure of crystal area in each sample.

2.10. Oil red O staining

Oil red O (ORO) (Sigma Aldrich, Oakville, ON) staining was performed as described previously [25]. Briefly, cells were fixed using 3% neutral buffered formalin for 40 min, followed by washing with dH2O and a 10 min pre-incubation with 60% isopropanol. A stock solution of ORO stain (0.5% *w*/*v* in isopropanol) was diluted 3:2 with dH2O and cells were exposed for 3–5 min at room temperature, followed by thorough washing with dH2O. ORO was extracted with 70% isopropanol and analyzed using a spectrophotometer at 510 nm wavelength.

2.11. Statistical analysis

One way ANOVA followed by a Tukey post test was used for multiple group pairwise comparisons. Unpaired t tests with Welch's correction were used when comparing two group means. Correlations between ER stress markers, ER-Chol, tissue cholesterol and inflammasome markers were analyzed by Pearson coefficient and by using non-linear regression with best fit to an exponential growth curve. All analyses were performed using GraphPad Prism V6.0 software.

3. Results

3.1. Wild type (WT) and *Ldlr* −/−*xLcat* +/+ mice are susceptible to HFHS diet-induced hepatic lipid accumulation and ER stress and *Ldlr* −/−*xLcat* −/− mice are protected from these phenotypes

Here we investigated the role of hepatocellular cholesterol in the development of fat rich diet-induced hepatic steatosis and hepatic ER stress by feeding the WT, *Ldlr* −/−*xLcat* +/+ and *Ldlr* −/−*xLcat* −/− mice a HFHS diet for 16 weeks. HFHS diet feeding resulted in significant increases in tissue neutral lipids (TG and CE) as well as free cholesterol (FC) in both WT and *Ldlr* −/−*xLcat* +/+ mice. In WT mice, we observed a 3.0-fold increase in TG, a 2.5-fold increase in CE and a 2.5-fold increase in FC. In *Ldlr* −/−*xLcat* +/+ mice, we observed a 2.2-fold increase in TG, 2.1-fold increase in CE and a 2.5-fold increase in FC (Fig. 1A–C). Both the WT mice and *Ldlr* −/−*xLcat* +/+ mice also showed induction of hepatic ER stress characterized by significant upregulation of *Chop* and *Xbp1s* mRNA expression (Fig. 1D,E), consistent with previous reports [21–23]. On the contrary, *Ldlr* −/−*xLcat* −/− mice resisted the increase in

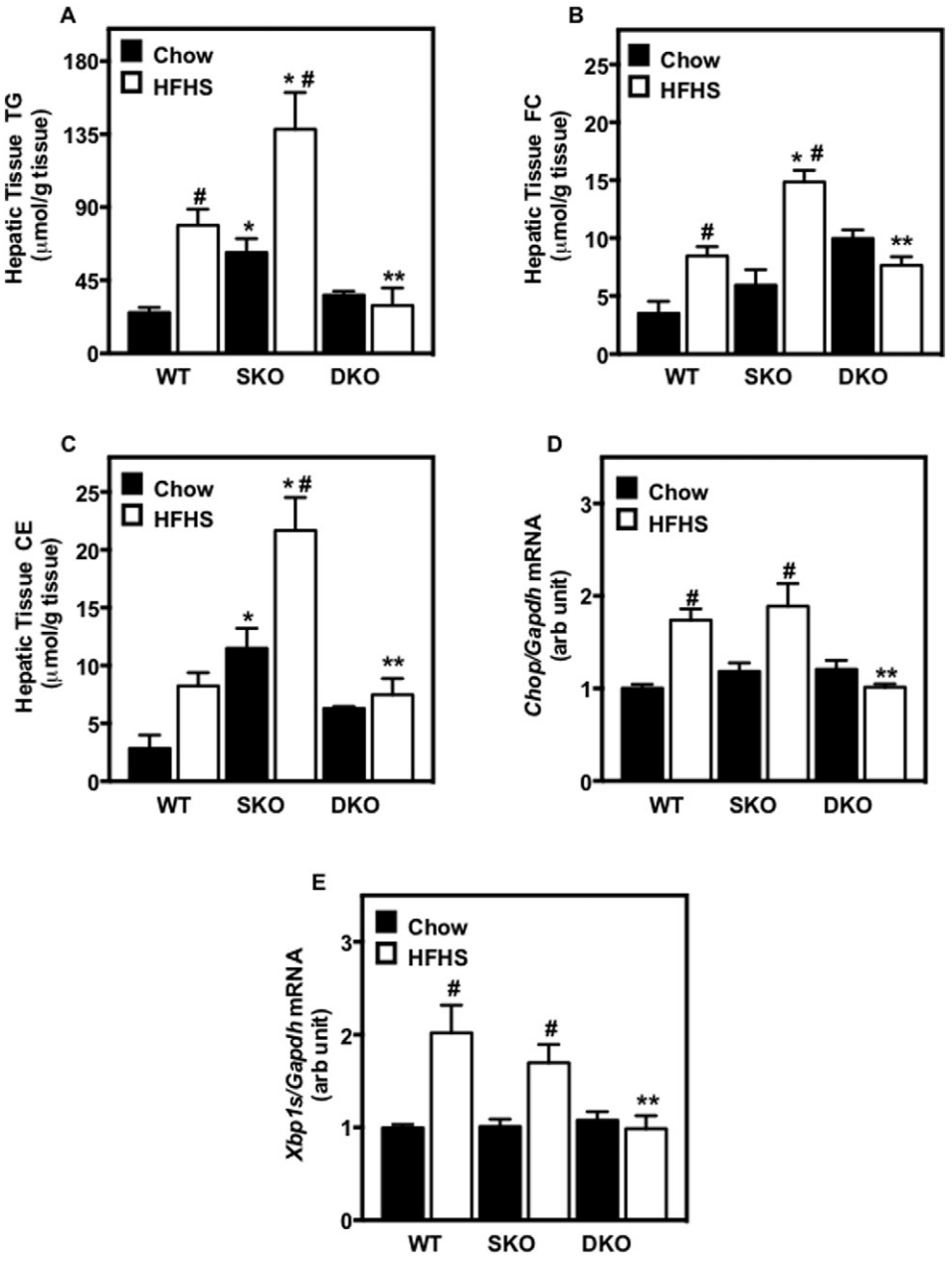

Fig. 1. Effect of HFHS diet on hepatic lipids and markers of hepatic ER stress. 10–12 week-old female WT, *Ldlr* −/−*xLcat* +/+ (SKO) and *Ldlr* −/−*xLcat* −/− (DKO) mice were fed either a chow or HFHS diet for 16 weeks and the effects of the two diets on (i) hepatic tissue lipids triglyceride (TG) (A), free cholesterol (FC) (B) and cholesterol ester (CE) (n = 4–5); (ii) mRNA levels of ER stress markers *Chop* (D) and *Xbp1s* (E) were compared. Data are means ± SE; #, $p < 0.05$ for pairwise comparison of HFHS-treated mice versus their respective chow fed controls; **, $p < 0.05$ for pairwise comparison of DKO versus SKO on the same diet by one-way ANOVA and Tukey post test.

all three tissue lipid fractions as well as induction of ER stress markers *Chop* and *Xbp1s* (Fig. 1A–E).

3.2. HFHS diet-induced hepatic cholesterol biosynthesis gene expression and excess ER cholesterol in WT and Ldlr −/−xLcat +/+ mice but not in Ldlr −/−xLcat −/− mice

We previously reported that *Ldlr* −/−*xLcat* +/+ mice being susceptible but *Ldlr* −/−*xLcat* −/− mice being resistant to ER membrane cholesterol accumulation and the corresponding hepatic ER stress in response to dietary cholesterol loading [19]. In order to investigate whether protection against HFHS diet-induced ER stress in *Ldlr* −/−*xLcat* −/− mice may also be related to protection from ER membrane cholesterol accumulation, we measured ER membrane FC and FC/PL ratio in WT, *Ldlr* −/−*xLcat* +/+ and *Ldlr* −/−*xLcat* −/− mice in response to this diet. HFHS diet feeding markedly increased ER PL and FC/PL ratio in WT and *Ldlr* −/−*xLcat* +/+ mice when compared to their respective chow fed controls (Fig. 2A,B). Of note is that ER PL levels are also increased in response to the HFHS diet feeding, in contrast to an absence of change in response to a high cholesterol diet as previously reported [20]. Furthermore, we observed a disproportionate increase in ER FC compared to the ER PL, as reflected by a higher fold increase in ER FC/PL ratio. In the case of *Ldlr* −/−*xLcat* −/− *mice*, this strain is resistant to the increase in each of these ER lipids and their ratio, which also correlated with the absence of increase in *Chop* and *Xbp1s* mRNA expression (Fig. 1D,E).

In the HFHS diet-induced ER stress model, we observed that hepatic *Chop* mRNA level correlates strongly with ER FC/PL ratio (Pearson r =

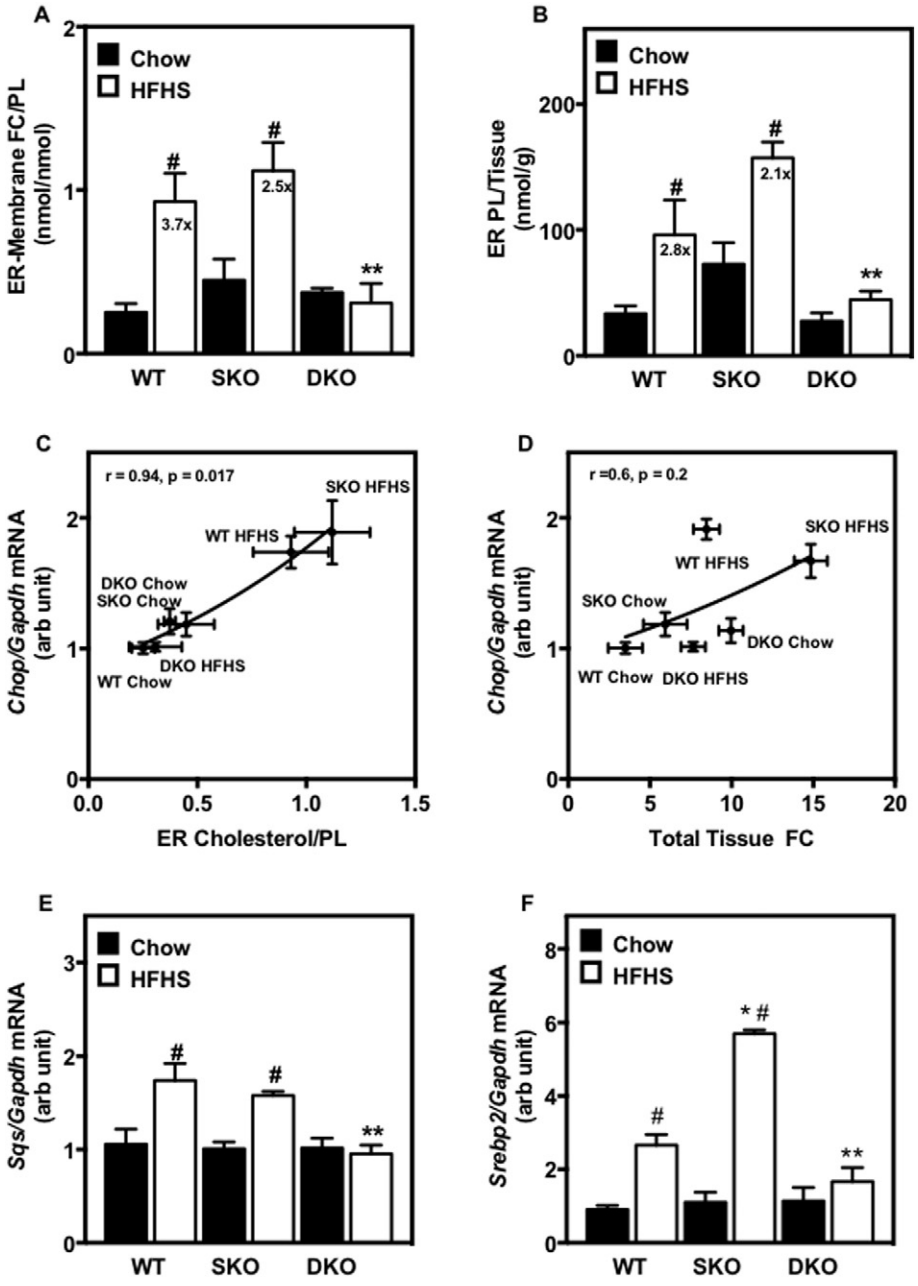

Fig. 2. Effect of HFHS diet on hepatic ER lipid species and cholesterol biosynthetic gene expression. 10–12 week old female WT, SKO and DKO mice were fed a chow or HFHS for 16 weeks. ER membrane fractions were isolated from liver tissues after an overnight fast. ER free cholesterol (FC) was measured by LC/MS/MS, and phospholipid (PL) was measured by colorimetric assay. Effect of HFHS diet vs chow fed controls on ER FC/PL (A) and ER PL(B) were analyzed for each mouse strain (n = 5 each). The correlation of ER stress marker *Chop* mRNA expression with ER FC/PL (C) and whole tissue FC (D) were analyzed. The solid line indicates the curve of best fit using an exponential non-linear regression analysis. Effect of HFHS diet on cholesterol biosynthetic genes mRNA expression, *Sqs* (E) and transcription factor *Srebp2* (F) were analyzed. Data are mean ± SE; #, $p < 0.05$ for pairwise comparison of HFHS diet-treated mice versus their respective chow fed controls; *, $p < 0.05$ for pairwise comparison of SKO versus WT on the same diet; **, $p < 0.05$ for pairwise comparison of DKO versus SKO on the same diet by one-way ANOVA and Tukey post test.

0.94, p = 0.02), but much less so with whole tissue FC (Spearman r = 0.6, p = 0.27) (Fig. 2C,D). These findings are consistent with our previous observation of selective positive correlation only for ER FC/PL but not whole tissue FC in the high dietary cholesterol feeding paradigm [20].

Earlier studies [15,26,27] suggest that high fat feeding in WT mice promoted activation of endogenous cholesterol biosynthesis in response to activation of SREBP2 processing. To determine whether this mechanism also applies to *Ldlr* −/−*Lcat* +/+ mice, in which hepatic cholesterol biosynthesis is already suppressed due to increased exogeneous cholesterol uptake and reduced biliary cholesterol efflux even under chow fed condition [20], we evaluated markers for endogenous cholesterol biosynthesis. We observed that HFHS diet induced mRNA expression of *Sqs* in both WT and *Ldlr* −/−*xLcat* +/+ mice by 1.8 and 1.6-fold, respectively but no change in *Ldlr* −/−*xLcat* −/− mice. Similarly, we also observed significant upregulation of *Srebp2* mRNA in WT and *Ldlr* −/−*xLcat* +/+ but not in *Ldlr* −/−*xLcat* −/− mice (Fig. 2E,F). Our findings in WT and *Ldlr* −/−*xLcat* +/+ suggest that HFHS diet feeding induces expression of cholesterol biosynthesis genes independent of their baseline expression and these changes are abrogated in the *Ldlr* −/−*xLcat* −/− mice, correlating with corresponding changes in ER-Chol and ER stress.

3.3. HFHS diet feeding induced hepatic NLRP3 inflammasome in WT and Ldlr −/−xLcat +/+ mice but not in Ldlr −/−xLcat −/− mice

Inflammasome activation plays an important role in the development of NASH. We investigated whether HFHS feeding induced NAFLD, in the context of hepatic lipid and hepatic ER-Chol accumulation, is directly linked to upregulation of NLRP3 inflammasome. We measured the mRNA expression of *Nlrp3* and *pro-Il-1β* in the same three strains of mice fed either a chow or HFHS diet. With 16 weeks of HFHS diet feeding, when compared to their respective chow fed controls, *Nlrp3* and *pro-Il-1β* mRNA were significantly increased in both WT and *Ldlr −/−xLcat +/+* mice by 2.0 fold each, but were unchanged in *Ldlr −/−xLcat −/−* mice (Fig. 3A,C). Hepatic IL1β protein levels in these mice also follow the same pattern of changes (Fig. 3E),

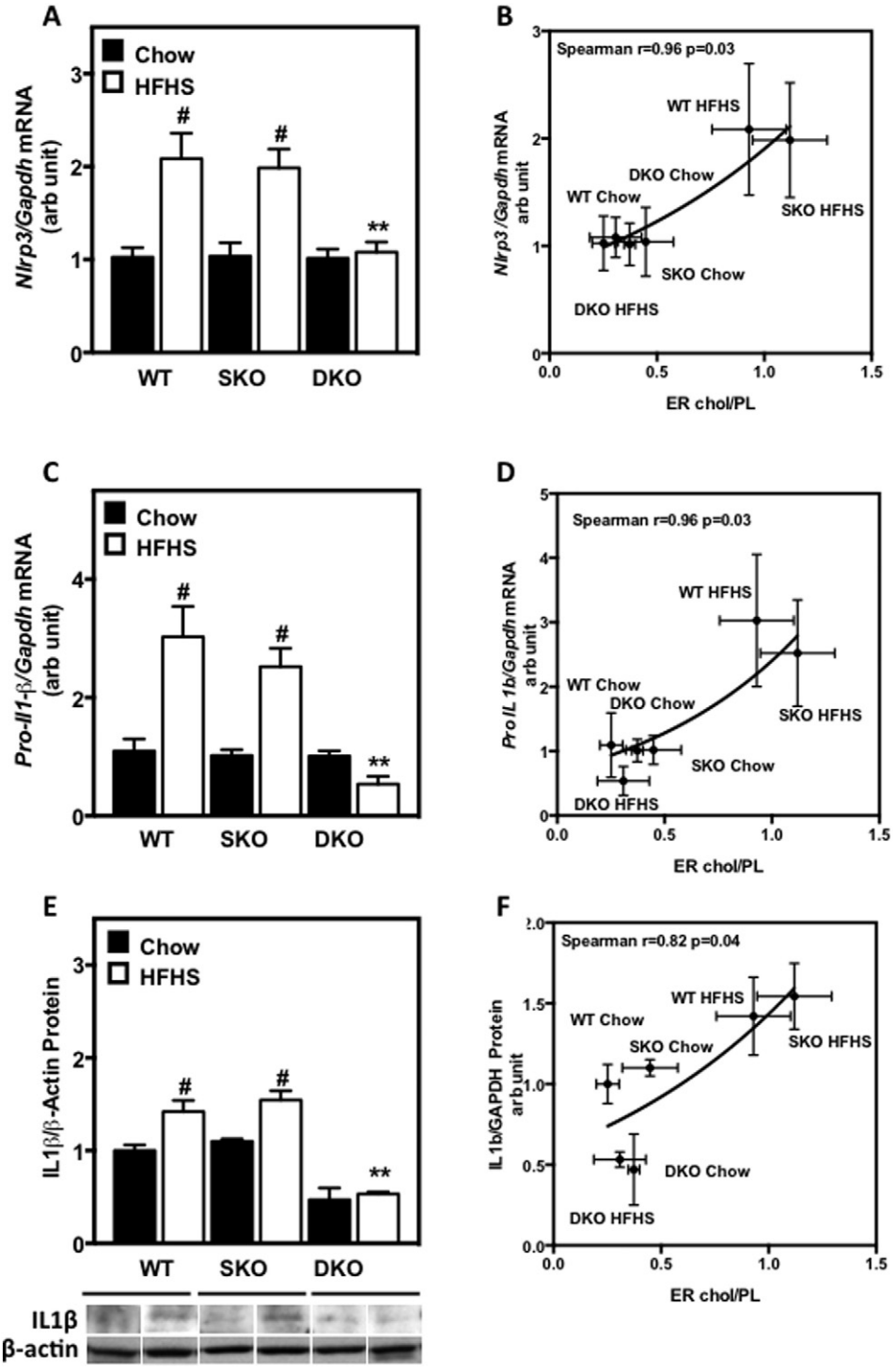

Fig. 3. Effect of HFHS diet on inflammasome markers gene expression. 10–12 week old female WT, SKO and DKO mice were fed a chow or HFHS diet for 16 weeks. Effect of the diet treatment on *Nlrp3* mRNA (*A*), *Pro-Il-1β* mRNA expressions (C) and IL1β protein (E) were analyzed. Representative Western blots were shown for each group. Data are mean ± SE; #, $p < 0.05$ for pairwise comparison of HFHS diet-treated mice vs their respective chow fed controls; **, $p < 0.05$ for pairwise comparison of DKO versus SKO on the same diet by one-way ANOVA and Tukey post test. Correlation between *Nlrp3* mRNA (B), *Pro-Il-1β* mRNA expression (D) and IL1β protein (F) versus ER FC/PL reported as Pearson coefficient (r). The solid line represents the curve of best fit using an exponential non-linear regression analysis.

establishing the consistency between mRNA levels of *Nlrp3* and *Pro-IL1β* and IL1β protein product, the latter previously shown to correlate with its circulating level [16]. The strong correlation of ER-Chol with ER stress (*Chop* mRNA) extends to that with *Nlrp3* mRNA, *Pro-IL1β* mRNA, and IL1β protein level with Pearson coefficient r being 0.96 ($p = 0.03$), 0.92 ($p = 0.01$) and 0.83 ($p = 0.04$), respectively (Fig. 3B,D,F).

3.4. *Ldlr −/− xLcat −/−* mice developed HCD-induced hepatic NLRP3 expression despite protection from ER cholesterol excess and ER stress

Recent study in our laboratory on the responses of these three mouse strains to the HCD revealed selective association between hepatic ER stress and ER-Chol but not whole tissue cholesterol, a relationship unmasked by the observation that *Ldlr −/− xLcat −/−* mice being

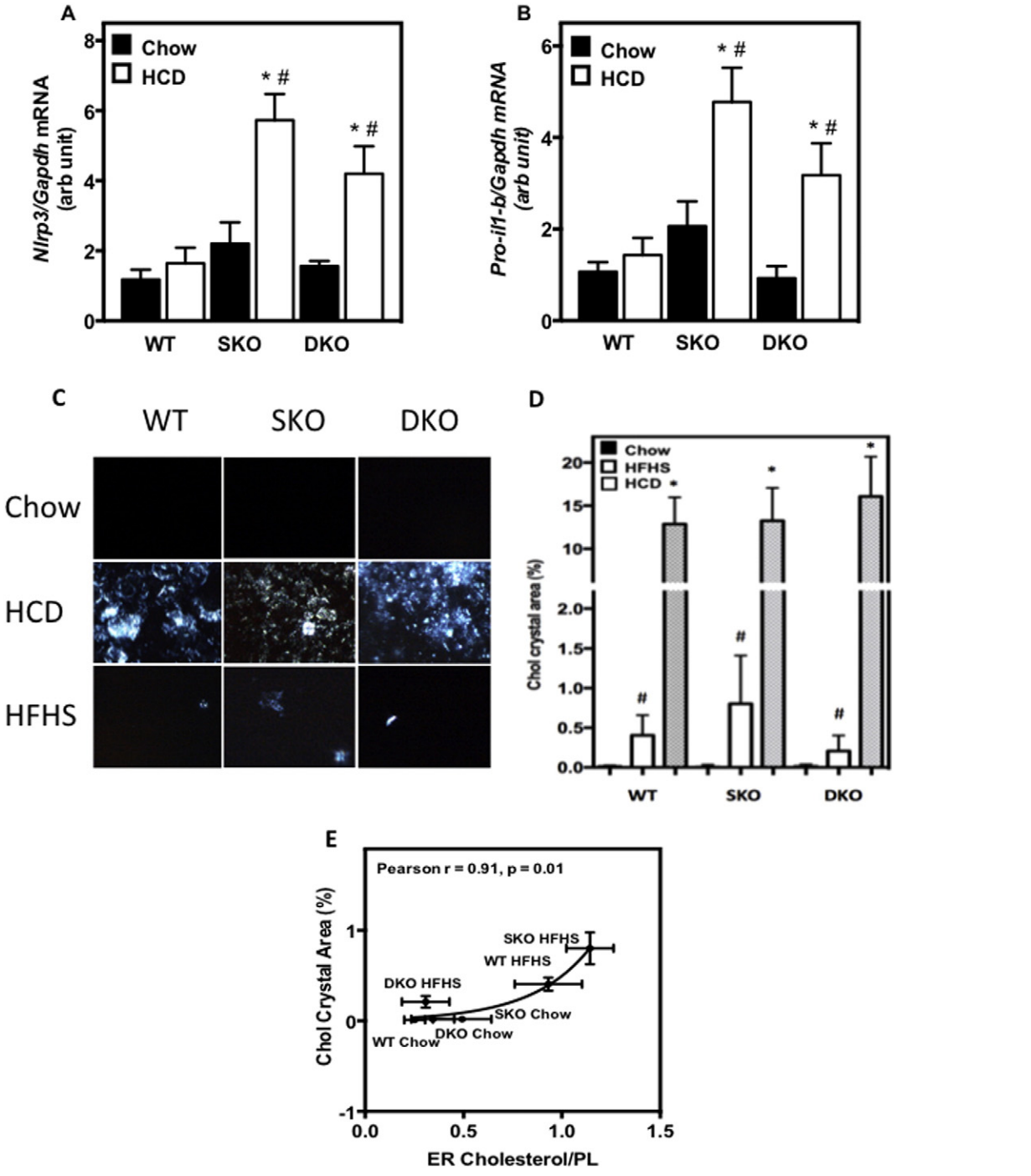

Fig. 4. Differential effects of HFHS and HCD on hepatic inflammasome gene expression and cholesterol crystal accumulation. 10–12 week old female WT, SKO and DKO mice were fed a 2%HCD for 10 weeks, a HFHS diet for 16 weeks and WT mice were fed the same two diets as controls. Expression of inflammasome genes *Nlrp3* mRNA (A) *and Pro-Il-1β* (B) mRNA expressions were analyzed. Data are mean ± SE. Analyses were one-way ANOVA and Tukey post test. *, $p < 0.05$ for pairwise comparison with their respective chow fed controls. **, $p < 0.05$ for pairwise comparison of DKO versus SKO on the same diet. (C) Representative images of birefringence from livers from WT, SKO and DKO each fed a chow, HCD and HFHS diet to illustrate abundance of cholesterol crystals. (D) Quantitation of cholesterol crystals pixel counts by ImageJ ($n = 10$ each for HFHS-fed mice and $n = 3$ each for HCD-fed mice). Analyses were one-way ANOVA and Tukey post test. # $p < 0.05$ for pairwise comparison of HFHS diet vs their respective chow fed controls; * $p < 0.05$ for pairwise comparison of HCD diet vs their respective chow fed controls. (E) Correlation between hepatic cholesterol crystal pixel counts versus ER FC/PL reported as Pearson coefficient (r). The solid line represents the curve of best fit using an exponential non-linear regression analysis.

protected from HCD-induced ER-Chol accumulation [20]. In light of the strong correlation between hepatic NLRP3 expression in response to the HFHS diet feeding with cholesterol biosynthetic gene expression, hepatic ER-Chol and ER stress markers, we investigated whether this correlation also applies in the same strains in response to the HCD diet. As seen in Fig. 4A and B, *Ldlr −/−xLcat +/+* mice showed significant induction of *Nlrp3* mRNA, as expected. However, in the case of *Ldlr −/−xLcat −/−*, in spite of protection from induction of ER-Chol and ER stress, this same diet also led significant induction of *Nlrp3* mRNA, suggesting the presence of inductive mechanisms independent of ER-Chol and ER stress.

3.5. Differential effect of HCD and HFHS diets on hepatic cholesterol crystal formation

To address whether the observed inflammasome activation may be linked to the presence of cholesterol crystals, we measured the latter by polarized light microscopy [12,13] and quantified abundance by surface area covered by birefringence signals. Similar to our previous report of HCD induced marked accumulation of total hepatic cholesterol in all three strains [20], we also observed substantial birefringence signals distributed inhomogeneously throughout the histologic sections, in comparison to nearly undetectable signals in all their respective chow-fed controls (Fig. 4C,D). Interestingly, unlike their HCD-fed counterparts, HFHS diet treatment resulted in considerably less induction of birefringence signals although the increase are still significant when compared to their respective chow-fed controls (Fig. 4D). Furthermore, the birefringent signal induction, though remaining significant, is considerably less in *Ldlr −/−xLcat −/−* mice than those of the WT and *Ldlr −/−xLcat +/+* mice (Fig. 4D).

We next investigated the relationship between ER FC/PL and birefringence signals under both diets. In HFHS- and chow-fed mice, the birefringence signals correlate strongly and positively with levels or ER FC/PL (Fig. 4E). By contrast, birefringence signals are substantially more abundant in all three strains fed the HCD (Fig. 4D), including the *Ldlr −/−xLcat −/−* mice, but correlate poorly with ER FC/PL (data not shown). Taken together, unlike their HFHS diet counterparts, HCD feeding resulted in (i) a more dramatic accumulation of cholesterol crystal which is inhomogeneously distributed, (ii) a significant but considerably more modest induction of NLRP3 in *Ldlr −/−xLcat −/−* mice in the absence of ER-Chol excess, suggesting that a fraction of the HCD-induced crystal accumulation might be accessible to pathways that activate NLRP3 inflammasomes.

3.6. Palmitate treatment dose-dependently induced steatosis and cholesterol biosynthesis in HepG2 cells

To further elucidate (i) the role of hepatocytes in the development of diet-induced NASH, independent of infiltrating macrophages and other resident cell types, and (ii) the relative role of exogenous saturated fatty acids and cholesterol, we employed a well-established cell model of saturated fatty acid-induced fatty liver. We first treated HepG2 cells with various doses of palmitate (0.3 mM, and 1.0 mM), a surrogate for excess dietary saturated fat, and established a dose-dependent increase in Oil red O staining (Fig. 5A).

In vivo studies in our laboratory (Fig. 2) and others [15] suggested that HFHS induced hepatic cholesterol accumulation occurs in part through de novo cholesterol biosynthesis (Fig. 2). Here, we test this hypothesis by treating HepG2 cells with palmitate at 0.3 mM for 16 h. In response to palmitate treatment, we observed significantly increased mRNA and protein expressions of *HMGR*, as well as *SQS*, another critical enzyme downstream in the mevalonate pathway (Fig. 5B–E) in association with an increase in cellular cholesterol levels and this increase in cholesterol was abrogated upon co-treatment with zaragozic acid (ZA), an inhibitor of SQS (Fig. 5F). The findings of increased expression of cholesterol biosynthesis genes are in agreement with previously published work, both in vivo and in vitro, showing a strong link between de novo cholesterol biosynthesis and the development of NAFLD [15,26,27].

3.7. Palmitate treatment of HepG2 cells recapitulates the correlation between cholesterol accumulation and induction of ER stress

In agreement with previous reports in the literature, we have also shown here that palmitate treatment of HepG2 cells increased gene expression of ER stress marker *CHOP* and *XBP1s* by 2.5 and 2-fold over controls, respectively (Fig. 6A,B). Similarly, co-treatment with ZA at 10 μM reversed palmitate-induced ER stress, shown as reduced gene expression of *CHOP* by 1.7-fold and *XBP1s* by 1.5-fold compared to palmitate treated cells (Fig. 6A,B). Furthermore, the reduced ER stress from inhibition of cholesterol biosynthesis with ZA was reversed with exogenous loading of cholesterol, supporting the primary role of cholesterol accumulation in the induction of ER stress, independent of its source (Fig. 6B).

3.8. Cholesterol biosynthesis and accumulation play important roles in palmitate-induced inflammasome activation in HepG2 cells

We next investigated whether palmitate treatment-induced cholesterol biosynthesis and accumulation also resulted in inflammasome activation in isolated hepatocytes. Palmitate treatment increased NLRP3 protein abundance by 1.5-fold and co-incubation of ZA ameliorated this effect (Fig. 7A). Similarly, palmitate treatment significantly induced protein expression of IL-1β and pro-IL-1β by 1.6 and 1.8-fold, respectively whereas co-incubation with ZA also normalized the expression of these cytokines (Fig. 7B,C). Although Elovl6, a target of Srebp1c, has been shown to be crucial in mediating the palmitate-induced inflammasome activation in hepatocytes [28], an absence of induction of the Elovl6 mRNA in response to palmitate treatment (data not shown) ruled out a significant role played by this enzyme, at least under the current experimental conditions. Taken together, our findings support the notion that accumulation of cellular cholesterol, irrespective of the source, is responsible for the upregulation of NLRP3 inflammasome and that either increased de novo biosynthesis per se or exogenous loading of cellular cholesterol is sufficient for activation in hepatocytes.

4. Discussion

In this study, we have shown for the first time that HFHS diet-induced hepatic *de novo* cholesterol biosynthesis is crucial for the development of hepatic ER stress and NLRP3 inflammasome activation in mice. We further provided supportive evidence that endogenously synthesized cholesterol is necessary for the activation of ER stress and inflammasome based on palmitate-treated HepG2 cell studies. On the other hand, a 2% high cholesterol diet per se can induce inflammasome activation independent of endogenous cholesterol synthesis, ER cholesterol and ER stress.

Our in vivo studies revealed that, in two susceptible strains, namely C57Bl/6 and *Ldlr −/−xLcat +/+* (in C57Bl/6 background), a 16-week HFHS diet feeding is sufficient to result in activation of both hepatic ER stress and NLRP3 inflammasome, the latter to include the tissue level of Caspase 1-processed IL-1β protein. Of note is that the fold-induction in both ER stress marker expression and NLRP3 inflammasome markers are comparable between the two strains, independent of LDL receptors deletion and its associated cellular cholesterol accumulation. On the contrary, in *Ldlr −/−xLcat −/−* mice, cholesterol biosynthesis gene expressions were unaltered by the diet and induction of both ER stress and inflammasome were abrogated. By employing the HepG2 cell model of saturated fatty acid-induced hepatocyte steatosis [29], our in vitro study also confirmed the primary importance of increase in cholesterol biosynthesis as source of cholesterol excess and in the induction ER stress and NLRP3 activation. Furthermore,

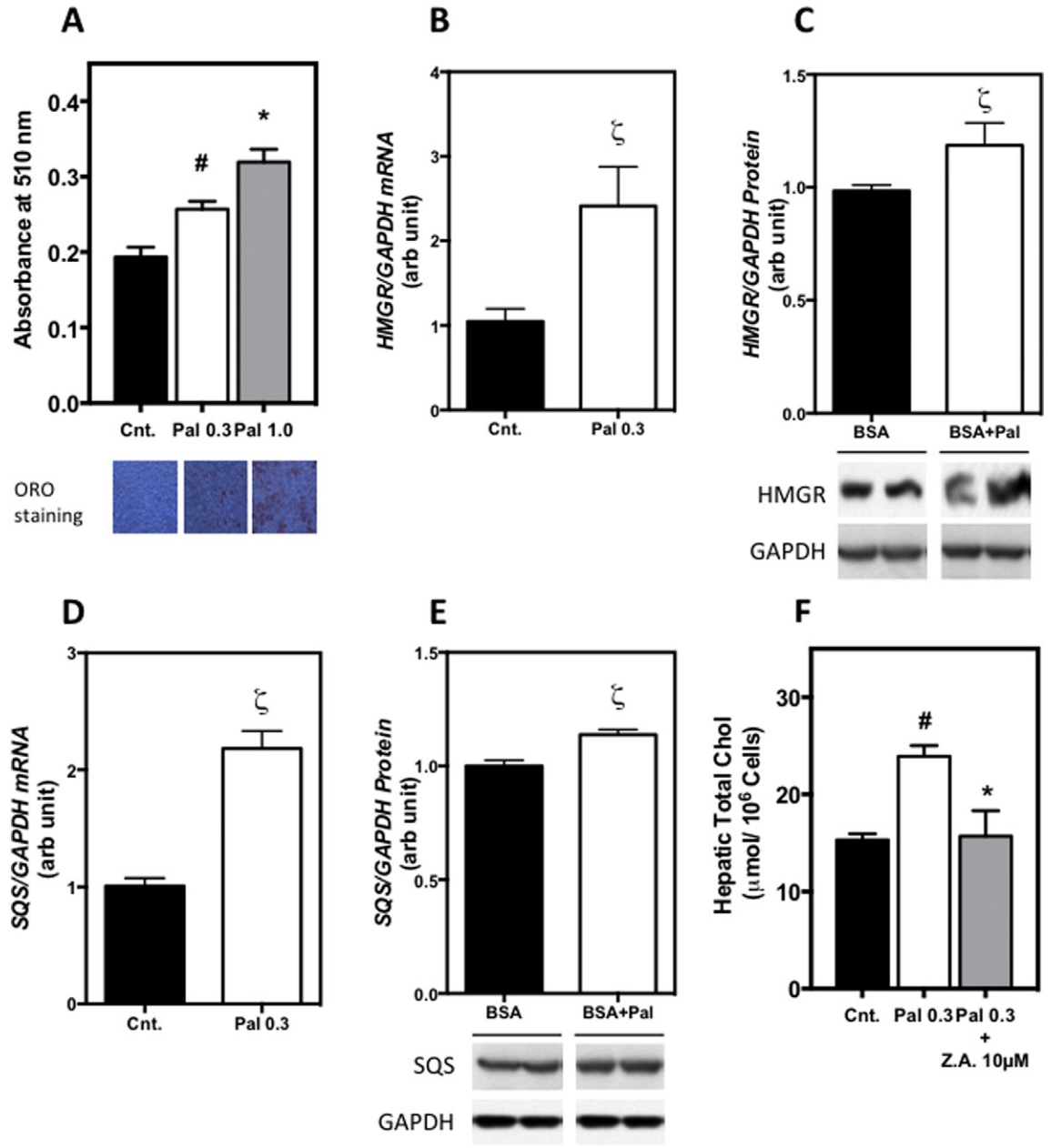

Fig. 5. The role of endogenous cholesterol biosynthetic pathway on palmitate-induced cholesterol accumulation in HepG2 cells. HepG2 cells were treated with palmitate 0.3 mM (Pal 0.3) and 1.0 mM (Pal 1.0) with or without zaragozic acid 10 μM (ZA 10 μM) for 16 h; A, Spectroscopic analysis at 510 nm (n = 8) and corresponding representative Oil red O stained sections, B, D, *HMGR* and *SQS* mRNA expression (n = 5), C, E, HMGR and SQS protein expression (n = 3–4) with representative Western blots from each treatment group showing duplicate bands from contiguous lanes, F, Total cholesterol measurement (n = 4). Data are mean ± SE; #, $p < 0.05$ for pairwise comparison of palmitate treated samples versus BSA (Cnt.); ζ, $p < 0.05$ for Student t-test, *, $p < 0.05$ for comparison of 0.3 mM palmitate treatment versus 1.0 mM palmitate (A) or versus 0.3 mM palmitate plus ZA treatment (F), with Mann–Whitney t-test for pairwise comparison or one-way ANOVA with Tukey post test for multiple comparison analysis.

supplementation of exogenous cholesterol was also found sufficient to activate both ER stress and NLRP3 in isolated hepatocytes even when endogenous cholesterol biosynthesis is inhibited. Note that, in our studies, a palmitate/BSA ratio of 6 was used which is similar to the ratio observed in humans immediately post-angioplasty (up to 7.5) [30], but whether it reflects the physiologic milieu in stable patients will require further elucidation.

By subjecting the same three mouse strains to the 2% HCD, we demonstrated a central role played by cellular cholesterol in the induction of hepatic steatosis and inflammasome activation. We showed that a 10-week HCD feeding resulted in induction of hepatic inflammasome activation not only in *Ldlr* −/−*xLcat* +/+ mice but also in *Ldlr* −/−*xLcat* −/− mice in spite of the latter being protected from hepatic ER-Chol accumulation and ER stress [20]. Likewise, this HCD also induces marked cholesterol crystal accumulation in all three strains. We have shown previously that, in the absence of HCD feeding, the cholesterol biosynthesis genes are suppressed in *Ldlr* −/−*xLcat* +/+ liver due to net increase in tissue cholesterol, but back to WT level in chow fed *Ldlr* −/−*Lcat* −/− mice. We therefore expect the expression of the biosynthesis genes in any strain, fed either a chow or HCD, should not exceed that of chow fed WT. Therefore, the HCD-induced cholesterol crystal accumulation and inflammasome activation are unlikely to be a result of increase in cholesterol biosynthesis but rather accumulation of exogenous cholesterol in the cell. The notion of cellular cholesterol excess being directly linked to induction of inflammasome activation is further supported by our in vitro observations that the ZA mediated

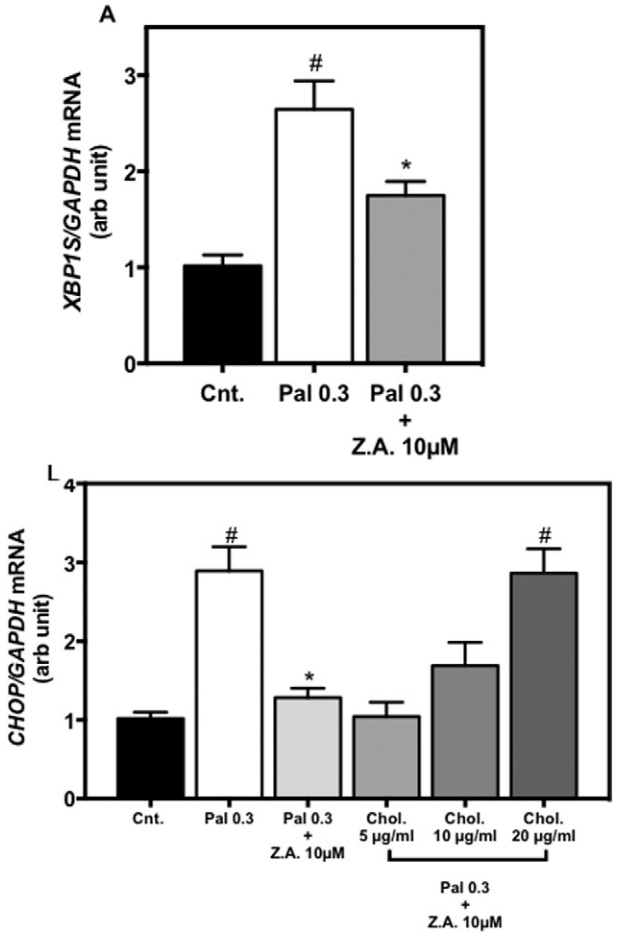

Fig. 6. Effect of endogenous cholesterol biosynthesis and exogenous cholesterol on palmitate-induced ER stress in HepG2 cells. HepG2 cells were treated with palmitate 0.3 mM (Pal 0.3) or BSA with or without concurrent treatment with squalene synthase zaragozic acid 10 μM (ZA 10 μM) or Cholesterol-MCD complex (5–20 μg/ml) for 16 h (n = 5). (A) Effect of ZA treatment on palmitate-induced *Xpb1s* mRNA expression; (B) Effect of ZA treatment on palmitate-induced *Chop* mRNA expression and its reversal by concurrent exogenous cholesterol loading. Data are mean ± SE. #, $p < 0.05$ for pairwise comparison of palmitate-treated samples versus BSA (Cnt.); *, $p < 0.05$ for pairwise comparison of ZA or cholesterol treated samples with palmitate-treated samples by one-way ANOVA, with Tukey post test.

suppression of inflammasomes may be overcome by exogenous cholesterol, putatively a result of activation by cholesterol in the non-ER compartments.

The presence of histological changes of inflammation is a cardinal feature of NASH. Evidence to support the importance of NLRP3 inflammasome in the development of NASH includes elevated levels of NLRP3 in liver biopsies of patients with NASH but not in those without [16,17]. In rodent model studies, Wree et al. reported near complete protection of prolonged choline-deficient, amino acid-defined (CDAA) diet-induced NASH in *Nlrp3* −/− mice [17]. Meanwhile, timed whole body over-expression of *Nlrp3* gene accelerates progression to NASH from simple steatosis in response to a short term CDAA feeding. On the other hand, the pathogenesis of NLRP3 activation remains incompletely understood. Here, we have provided direct in vivo and in vitro evidence that cholesterol accumulation, independent of its origin, increased tissue expression of NLRP3 and IL-1β, the latter a surrogate for the circulating IL-1β. In the HFHS diet studies, we observed striking correlations between hepatic ER stress, markers of inflammasome activation and cholesterol crystal abundance with ER-Chol, raising the possibility that the de novo synthesis of cholesterol may be rate limiting for the inflammasome activation as a result of accumulation cholesterol crystal and ER-Chol, the latter via induction of ER stress through dysfunction of sarco/endoplasmic reticulum Ca^{2+}-ATPase [31]. However, further studies are required to firmly establish a mechanistic link between ER stress and inflammasome activation in the liver and to resolve the relative contribution of the two forms of cholesterol accumulation.

Based on our findings, the potential role of cellular cholesterol in the activation of NLRP3 inflammasome is distinctly different between high fat and high cholesterol diets. In the HFHS diet feeding paradigm, the dependency of inflammasome activation parallels that of ER stress and cholesterol biosynthesis. This relationship is also recapitulated in the in vitro studies, namely inhibition of cholesterol biosynthesis with zaragozic acid directly suppresses the expression of markers of inflammasome. Mechanistically, increased cholesterol biosynthesis in the ER could potentially raise the abundance of FC in the lipid droplets [32]. This may in turn result in accumulation of cholesterol crystal, a known activator of NLRP3 inflammasome. The possibility of intracellular nucleation of cholesterol crystal has previously been demonstrated in models of macrophages [33,34]. The detection of diffuse distribution of crystals in all three strains in response to HFHS diet-fed is consistent with this notion. However, in light of the positive correlation between inflammation marker expression and cholesterol crystal levels, the relative low degree of induction of crystal formation in *Ldlr* −/− *xLcat* −/− and the absence of significant inflammasome activation in this strain suggest existence of a threshold level of cholesterol accumulation. Further experiments are needed to further elucidate this hypothesis. On the other hand, feeding mice with a 2% HCD effectively induces steatosis and inflammasome activation in *Ldlr* −/− *xLcat* −/− mice despite being protected from ER-Chol accumulation and ER stress, suggestive of distinct alternate pathways in mediating dietary cholesterol induced inflammasome activation. Previous studies demonstrated that extracellular cholesterol crystal activates inflammasome indirectly via cellular uptake, internalization and conversion into cholesterol ester before promoting leakage of lysosomal cathepsin B [33]. It is conceivable that the dietary cholesterol from remnant uptake may contribute to inflammasome activation by similar pathways. Meanwhile, McARH7777 cells treated with exogenous cholesterol or fatty acids have been shown to accumulate CE-enriched and TG-enriched lipid droplets differentially, in association with specific members of the perilipin family [35]. It is therefore conceivable that cholesterol from distinct pools of lipid droplets may differentially contribute to the activation of inflammasome, in part accounting for the differential response between WT and *Ldlr* −/− *xLcat* −/− mice. The relatively modest degree of induction of inflammasome in relation to the dramatic induction of birefringent signal by the diet may reflect partial sequestration of the cholesterol crystals. Further studies are required to test this putative mechanism.

5. Conclusion

Our combined in vivo and in vitro studies have provided mechanistic insight into the role of cellular cholesterol in the development of diet-induced NASH in part through promotion of inflammasome activation. We have provided compelling evidence that fat- and cholesterol-rich diets engage distinct and yet complementary pathways in the accumulation of cellular cholesterol in selective compartments, potentially accounting for the synergistic action of these two dietary ingredients in the development of NASH. Our findings may provide a novel cholesterol-focused framework for future development of novel therapeutic strategies for the prevention and treatment of NASH.

Conflict of interest

None of the authors have any conflict of interest.

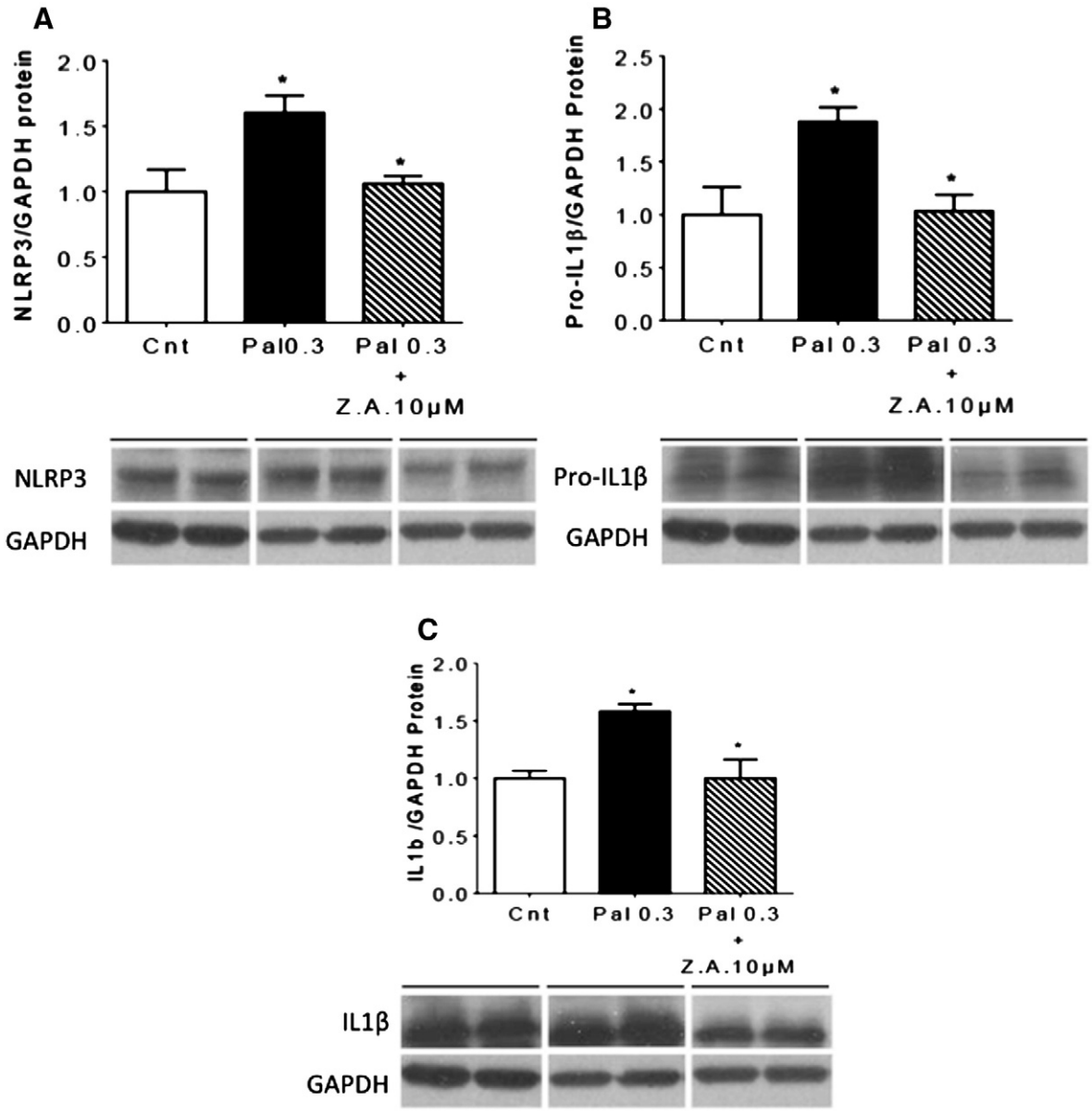

Fig. 7. Effect of ZA treatment on palmitate-induced inflammasomes protein levels. (A–C) HepG2 cells were treated with 0.3 mM palmitate (Pal 0.3) with or without zaragozic acid 10 μM (ZA 10 μM) (n = 4) for 16 h. Cellular levels of NLRP3, pro-IL-1β, IL-1β proteins were measured by Western blot. Anti-ProIL-1β was used to detect both IL-1β (35KDa) and pro-IL-1β (17KDa). Representative Western blots from each treatment group were shown as duplicate bands from contiguous lanes. Data are mean ± SE; #, $p < 0.05$ for pairwise comparison of palmitate treated samples versus BSA (Cnt.); *,$p < 0.05$ for pairwise comparison of ZA treated samples with palmitate treated samples by one-way ANOVA, with Tukey post test.

Transparency document

The transparency document associated with this article can be found, in online version.

Acknowledgments

This study has been supported by a Banting & Best Diabetes Centre Fellowship in Diabetes Care (Funded by Eli Lilly and Boehringer Ingelheim) to Dinushan Nesan. We thank Drs Allen Volchuk and Phil Connelly for their critical review of the manuscript.

Grants: This work was supported in part by a Canadian Institutes of Health Research operating grant (MOP 275369) and a China–Canada Joint Health Research Initiative grant (FRN109621) to D.S. Ng, a Grant-in-Aid from the Heart and Stroke Foundation of Canada (G-13-00026) to C.L. Cummins and (G-15-0009340) to K. Adeli.

References

[1] P. Angulo, Non-alcholic fatty liver disease, N. Engl. J. Med. 346 (2002) 1221–1232.
[2] J.D. Browning, J.D. Horton, Molecular mediators of hepatic steatosis and liver injury, J. Clin. Invest. 114 (2004) 147–152.
[3] J.D. Browning, L.S. Szczepaniak, R. Dobbins, P. Nuremberg, J.D. Horton, J.C. Cohen, S.M. Grundy, H.H. Hobbs, Prevalence of hepatic steatosis in an urban population in the United States: impact of ethnicity, Hepatology 40 (2004) 1387–1395.
[4] D.E. Kleiner, E.M. Brunt, Nonalcoholic fatty liver disease: pathologic patterns and biopsy evaluation in clinical research, Semin. Liver Dis. 32 (1) (2012) 3–13.
[5] E.M. Brunt, D.E. Kleiner, L.A. Wilson, P. Belt, B.A. Neuschwander-Tetri, NASH clinical research network (CRN), nonalcoholic fatty liver disease (NAFLD) activity score and the histopathologic diagnosis in NAFLD: distinct clinicopathologic meanings, Hepatology 53 (3) (2011) 810–820.
[6] H.-K. Min, A. Kapoor, M. Fuchs, F. Mirshahi, H. Zhou, J. Maher, J. Kellum, R. Warnick, M.J. Contos, A.J. Sanyal, Increased hepatic synthesis and dysregulation of cholesterol metabolism is associated with the severity of nonalcoholic fatty liver disease, Cell Metab. 15 (2013) 1–3.
[7] A.K. Leamy, R.A. Egnatchik, J.D. Young, Molecular mechanisms and the role of saturated fatty acids in the progression of non-alcoholic fatty liver disease, Prog. Lipid Res. 52 (1) (2013) 165–174.

[8] C.C. Duwaerts, J.J. Maher, Mechanisms of liver injury in non-alcoholic steatohepatitis, Curr. Hepatol. Rep. 13 (2) (2014) 119–129.
[9] G. Arguello, E. Balboa, M. Arrese, S. Zanlungo, Recent insights on the role of cholesterol in non-alcoholic fatty liver disease, Biochim. Biophys. Acta 1852 (2015) 1765–1778.
[10] P. Puri, R.A. Baillie, M.M. Wiest, F. Mirshahi, J. Choudhury, O. Cheung, C. Sargeant, M.J. Contos, A.J. Sanyal, A lipidomic analysis of nonalcoholic fatty liver disease, Hepatology 46 (2007) 1081–1090.
[11] C. Savard, E.V. Tartaglione, R. Kuver, W.G. Haigh, G.C. Farrell, S. Subramanian, A. Chait, M.M. Yeh, L.S. Quinn, G.N. Ioannou, Synergistic interaction of dietary cholesterol and dietary fat in inducing experimental steatohepatitis, Hepatology 57 (2013) 81–92.
[12] G.N. Ioannou, H.W. Geoffrey, T. David, C. Savard, Hepatic cholesterol crystals and crown-like structures distinguish NASH from simple steatosis, J. Lipid Res. 54 (2013) 1326–1334.
[13] G.N. Ioannou, D.M. van Rooyen, C. Savard, W.G. Haigh, M.M. Yeh, N.C. Teoh, G.C. Farrell, Cholesterol-lowering drugs cause dissolution of cholesterol crystals and disperse Kupffer cell crown-like structures during resolution of NASH, J. Lipid Res. 56 (2015) 277–285.
[14] V. Bieghs, P.J. Van Gorp, K. Wouters, T. Hendrikx, M.J. Gijbels, M. van Bilsen, J. Bakker, C.J. Binder, D. Lütjohann, B. Staels, M.H. Hofker, R. Shiri-Sverdlov, LDL receptor knock-out mice are a physiological model particularly vulnerable to study the onset of inflammation in non-alcoholic fatty liver disease, PLoS ONE 7 (1) (2012), e30668.
[15] N. Wu, L.K. Sarna, S.Y. Hwang, Q. Zhu, P. Wang, Y.L. Siow, K. O, Activation of 3-hydroxy-3-methylglutaryl coenzyme A (HMG-CoA) reductase during high fat diet feeding, Biochim. Biophys. Acta 1832 (2013) 1560–1568.
[16] T. Csak, M. Ganz, J. Pespisa, K. Kodys, A. Dolganiuc, G. Szabo, Fatty acid and endotoxin activate inflammasomes in mouse hepatocytes that release danger signals to stimulate immune cells, Hepatology 54 (2011) 133–144.
[17] A. Wree, M.D. McGeough, C.A. Peña, M. Schlattjan, H. Li, M.E. Inzaugarat, K. Messer, A. Canbay, H.M. Hoffman, A.E. Feldstein, NLRP3 inflammasome activation is required for fibrosis development in NAFLD, J. Mol. Med. (Berl) 92 (10) (2014) 1069–1082.
[18] C.M. Oslowski, T. Hara, B. O'Sullivan-Murphy, K. Kanekura, S. Lu, M. Hara, S. Ishigaki, L.J. Zhu, E. Hayashi, S.T. Hui, D. Greiner, R.J. Kaufman, R. Bortell, F. Urano, Thioredoxin-interacting protein mediates ER stress-induced β cell death through initiation of the inflammasome, Cell Metab. 16 (2) (2012) 265–273.
[19] D.S. Ng, The role of lecithin:cholesterol acyltransferase in the modulation of cardiometabolic risks — a clinical update and emerging insights from animal models, Biochim. Biophys. Acta 1821 (4) (2012) 654–659.
[20] L. Hager, L. Li, H. Pun, L. Liu, M.A. Hossain, G.F. Maguire, M. Naples, C. Baker, L. Magomedova, J. Tam, K. Adeli, C.L. Cummins, P.W. Connelly, D.S. Ng, Lecithin:cholesterol acyltransferase deficiency protects against cholesterol-induced hepatic endoplasmic reticulum stress in mice, J. Biol. Chem. 287 (2012) 20755–20768.
[21] L. Li, M.A. Hossain, S. Sadat, L. Hager, L. Liu, L. Tam, S. Schroer, L. Huogen, I.G. Fantus, P.W. Connelly, M. Woo, D.S. Ng, Lecithin cholesterol acyltransferase null mice are protected from diet-induced obesity and insulin resistance in a gender-specific manner through multiple pathways, J. Biol. Chem. 286 (2011) 17809–17820.
[22] U. Ozcan, Q. Cao, E. Yilmaz, A.-H.H. Lee, N.N. Iwakoshi, E. Ozdelen, G. Tuncman, C. Görgün, L.H. Glimcher, G.S. Hotamisligil, C. Gorgun, Endoplasmic reticulum stress links obesity, insulin action, and type 2 diabetes, Science 306 (2004) 457–461.
[23] U. Ozcan, E. Yilmaz, L. Ozcan, M. Furuhashi, E. Vaillancourt, R.O. Smith, C.Z. Görgün, G.S. Hotamisligil, Chemical chaperones reduce ER stress and restore glucose homeostasis in a mouse model of type 2 diabetes, Science 313 (2006) 1137–1140.
[24] K.J. Livak, T.D. Schmittgen, Analysis of relative gene expression data using realtime quantitative PCR and the 2ΔΔC(T) method, Methods 25 (4) (2001) 402–408.
[25] K. Funai, H. Song, L. Yin, I.J. Lodhi, X. Wei, J. Yoshino, T. Coleman, C.F. Semenkovich, Muscle lipogenesis balances insulin sensitivity and strength through calcium signaling, J. Clin. Invest. 123 (2013) 1229–1240.
[26] T.V. Fungwe, J.E. Fox, L.M. Cagen, H.G. Wilcox, M. Heimberg, Stimulation of fatty acid biosynthesis by dietary cholesterol and of cholesterol synthesis by dietary fatty acid, J. Lipid Res. 35 (1994) 311–318.
[27] E.H. Goh, M. Heimberg, Effects of free fatty acids on activity of hepatic microsomal 3-hydroxy-3-methylglutaryl coenzyme a reductase and on secretion of triglyceride and cholesterol by liver, J. Biol. Chem. 252 (1977) 2822–2826.
[28] T. Matsuzaka, A. Atsumi, R. Matsumori, T. Nie, H. Shinozaki, N. Suzuki-Kemuriyama, M. Kuba, Y. Nakagawa, K. Ishii, M. Shimada, K. Kobayashi, M. Yatoh, A. Takahashi, K. Takekoshi, H. Sone, N. Yahagi, H. Suzuki, S. Murata, M. Nakamuta, N. Yamada, H. Shimano, Elovl6 promotes nonalcoholic steatohepatitis, Hepatology 56 (2012) 2199–2208.
[29] Y. Zhang, M.L. Chen, Y. Zhou, L. Yi, Y.X. Gao, L. Ran, S.H. Chen, T. Zhang, X. Zhou, D. Zou, B. Wu, Y. Wu, H. Chang, J.D. Zhu, Q.Y. Zhang, M.T. Mi, Resveratrol improves hepatic steatosis by inducing autophagy through the cAMP signaling pathway, Mol. Nutr. Food Res. 59 (8) (2015) 1443–1457.
[30] A.M. Kleinfeld, D. Prothro, D.L. Brown, R.C. Davis, G.V. Richieri, A. DeMaria, Increases in serum unbound free fatty acid levels following coronary angioplasty, Am. J. Cardiol. 78 (12) (1996) 1350–1354.
[31] S. Fu, L. Yang, P. Li, O. Hofmann, L. Dicker, W. Hide, X. Lin, S.M. Watkins, A.R. Ivanov, G.S. Hotamisligil, Aberrant lipid metabolism disrupts calcium homeostasis causing liver endoplasmic reticulum stress in obesity, Nature 473 (7348) (2011) 528–531.
[32] A.R. Thiam, R.V. Farese Jr., T.C. Walther, The biophysics and cell biology of lipid droplets, Nat. Rev. Mol. Cell Biol. 14 (12) (2013) 775–786.
[33] K. Rajamäki, J. Lappalainen, K. Oörni, E. Välimäki, S. Matikainen, P.T. Kovanen, K.K. Eklund, Cholesterol crystals activate the NLRP3 inflammasome in human macrophages: a novel link between cholesterol metabolism and inflammation, PLoS ONE 5 (7) (2010), e11765.
[34] F.J. Sheedy, A. Grebe, K.J. Rayner, P. Kalantari, B. Ramkhelawon, S.B. Carpenter, C.E. Becker, H.N. Ediriweera, A.E. Mullick, D.T. Golenbock, L.M. Stuart, E. Latz, K.A. Fitzgerald, K.J. Moore, CD36 coordinates NLRP3 inflammasome activation by facilitating intracellular nucleation of soluble ligands into particulate ligands in sterile inflammation, Nat. Immunol. 14 (8) (2013) 812–820.
[35] K. Hsieh, Y.K. Lee, C. Londos, B.M. Raaka, K.T. Dalen, A.R. Kimmel, Perilipin family members preferentially sequester to either triacylglycerol-specific or cholesteryl-ester-specific intracellular lipid storage droplets, J. Cell Sci. 125 (Pt 17) (2012) 4067–4076.